

# Cluster-based Input Weight Initialization for Echo State Networks

Peter Steiner, Azarakhsh Jalalvand *Member, IEEE*, Peter Birkholz, *Member, IEEE*

**Abstract**—Echo State Networks (ESNs) are a special type of recurrent neural networks (RNNs), in which the input and recurrent connections are traditionally generated randomly, and only the output weights are trained. Despite the recent success of ESNs in various tasks of audio, image and radar recognition, we postulate that a purely random initialization is not the ideal way of initializing ESNs. The aim of this work is to propose an unsupervised initialization of the input connections using the  $K$ -Means algorithm on the training data. We show that this initialization performs equivalently or superior than a randomly initialized ESN whilst needing significantly less reservoir neurons (2000 vs. 4000 for spoken digit recognition, and 300 vs. 8000 neurons for  $f_0$  extraction) and thus reducing the amount of training time. Furthermore, we discuss that this approach provides the opportunity to estimate the suitable size of the reservoir based on the prior knowledge about the data.

**Index Terms**—Echo State Networks, Reservoir computing, speech recognition, clustering algorithms.

## I. INTRODUCTION

Since the breakthrough of ESNs [1], a lot of design strategies for ESNs have been proposed. Although randomly initialized ESNs have achieved state-of-the-art results in various directions, several publications, such as [2]–[4] argue that there should exist better approaches that incorporate more prior or biologically plausible knowledge. According to [5], it requires a lot of trial and error to initialize an ESN for a task, and the relationship between the different weight matrices is not completely understood.

As a result, various design strategies for ESNs have been proposed and evaluated. To better understand the behavior of randomly initialized ESNs for digit and phoneme recognition, Jalalvand et. al. [6], [7] have analyzed an ESN with optimized hyper-parameters and determined the hyper-parameters together with an optimization strategy that it is adopted here. For example, it turned out that even very sparse weight matrices are still sufficient for achieving proper results.

Other approaches step even farther away from random initialization. The publications [8]–[10] proposed *simple* ESN reservoirs in different flavors, e.g. delay lines with optional feedback, cyclic reservoirs, or even a simple chain of neurons. It was shown that the proposed reservoir design strategies

outperformed randomly initialized ESNs in various aspects, such as classification or regression accuracy and in terms of memory capacity. A big advantage is a relatively high sparsity, which is memory-efficient and computationally cheap. However, at least in [9], the authors warn that their findings might not hold in practice, when one needs to deal with high-dimensional inputs or more complex tasks. A related approach to simplify the reservoir initialization is proposed in [11], where the reservoir weights are only allowed to have the values 0 and  $\pm 1$ . Starting with the values 1 and 0, which were assigned to the reservoir in a deterministic way, several 1 weights were flipped to  $-1$  and the authors have shown that this strongly influenced the behaviour of the reservoir in terms of fitting error and memory capacity. In [12], the aforementioned approaches were further simplified, and only one neuron was used in the reservoir. The output of the neuron was fed back to its input using different delay times. This produced virtual nodes that simulated a larger reservoir.

All these pioneering approaches try to initialize the reservoir and/or input weights in a more or less deterministic way that is almost task-independent. Alternative techniques also aim to initialize the ESN in a deterministic way that is, however, more task-dependent or dependent on the input data. For example, [13] adopted recurrent self-organizing maps (SOMs) to initialize the input and recurrent weight matrices using the SOM algorithm. Therefore, a new neuron model was used, and the weight matrices were pre-trained using the unsupervised SOM algorithm. In [14] scale-invariant maps (SIMs), an extension of SOMs, were used to initialize the input weights. The same group also used Hebbian learning in [15]. Lazar et. al. [16] proposed a biologically-inspired self-organizing recurrent neural network (SORN) consisting of spiking neuron models, in which the weights of frequently firing neurons are getting increased during training. This was adopted for the Batch Intrinsic Plasticity (BIP) for ESNs [17], where the reservoir weights were iteratively pre-trained.

Yet another family of unsupervised learning algorithms are clustering techniques. In [18], the Inverse Weighted  $K$ -Means (IWK) algorithm [19], [20] was proposed to initialize the weight matrices of an ESN. After randomly initializing the input weights, they applied IWK to the neuron inputs and adapted the input weights. Then they randomly initialized the recurrent weights and applied IWK again on the reservoir states to adapt the recurrent weights. The authors showed that their method outperformed a randomly initialized ESN and the performance gets more stable when repeating random initialization.

In this paper, we present an alternative strategy to initialize the ESN with the  $K$ -Means algorithm. Instead of applying the

This research was financed by Europäischer Sozialfonds (ESF), the Free State of Saxony (Application number: 100327771), and Special Research Fund of Ghent University (BOF19/PDO/134). (*Corresponding author: Peter Steiner*)

P. Steiner and P. Birkholz are with the Institute for Acoustics and Speech Communication, Technische Universität Dresden, 01069 Dresden, Germany, (e-mail: peter.steiner@tu-dresden.de; peter.birkholz@tu-dresden.de)

Azarakhsh Jalalvand is with IDLab, Ghent University, Belgium, as well as Mechanical and Aerospace Engineering department, Princeton University, USA (email: azarakhsh.jalalvand@ugent.be)

Manuscript received MONTH XX, 2021; revised MONTH XX, 2021.

cluster algorithm on the neuron inputs, we used the  $K$ -Means algorithm to cluster the *input features* and used the centroid vectors as input weights.

The main advantages of our approach are:

- The pre-trained ESNs perform equally well or better than ESNs without pre-training and need smaller reservoirs. This will be discussed for two real-world problems, namely, spoken digit recognition and  $f_0$  extraction from speech signals.
- We show that the same hyper-parameter optimization strategy proposed in [6], [7] for conventional ESNs can be applied to optimize the hyper-parameters of the novel  $K$ -Means-based initialized ESN (KM-ESN).
- Applying clustering techniques is a common data exploration step to study possible correlations within the data. Our approach efficiently benefits from the outcome of this step to also initialize the input weights.
- Since the clusters are usually associated with the classes to be recognized, e.g. phones in speech or notes in music, the procedure of our approach is interpretable.

The remainder of this paper is structured as follows: In Section II, we introduce the basic ESN and our proposed unsupervised input weight initialization. In Section III, we introduce, optimize and evaluate ESNs for spoken digit classification. In Section IV, we present results on  $f_0$  extraction using ESNs on a large-scale dataset. Finally, we summarize our conclusions and give an outlook to future work in Section V.

## II. METHODS

Here, we give an introduction of a basic ESN, introduce the  $K$ -Means algorithm and explain how the input weights of an ESN can be initialized using the  $K$ -Means algorithm.

### A. Basic Echo State Network

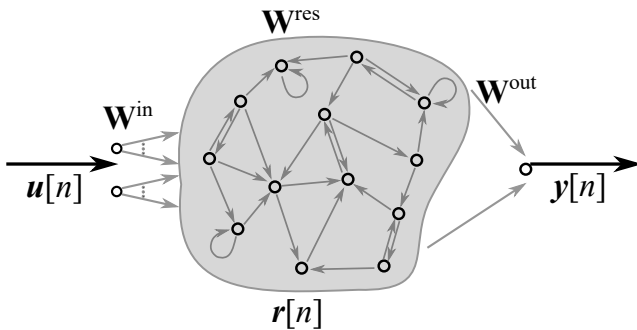


Fig. 1. Main components of a basic ESN: The input features  $u[n]$  are fed into the reservoir using the fixed input weight matrix  $W^{in}$ . The reservoir consists of unordered neurons, sparsely inter-connected via the fixed reservoir matrix  $W^{res}$ . The output  $y[n]$  is a linear combination of the reservoir states  $r[n]$  based on the output weight matrix  $W^{out}$ , which is trained using linear regression.

The main outline of a basic ESN is depicted in Fig. 1. The model consists of the input weights  $W^{in}$ , the reservoir weights  $W^{res}$  and the output weights  $W^{out}$ . The input weight matrix  $W^{in}$  has the dimension of  $N^{res} \times N^{in}$ , where  $N^{res}$  and  $N^{in}$

are the size of the reservoir and dimension of the input feature vector  $u[n]$  with the time index  $n$ , respectively. Typically, the values inside the input weight matrix are initialized randomly from a uniform distribution between  $\pm 1$  and are scaled afterwards using the input scaling factor  $\alpha_u$ , which is a hyper-parameter to be tuned. In [6], it was shown that it is sufficient to have only a limited number of connections from the input nodes to the nodes inside the reservoir. We therefore connect each node of the reservoir to only  $K^{in} = 10$  ( $\ll N^{in}$ ) randomly selected input features. This makes  $W^{in}$  very sparse and feeding the feature vectors into the reservoir potentially more efficient.

The reservoir weight matrix  $W^{res}$  is a square matrix of the size  $N^{res} \times N^{res}$ . Typically, the values inside this matrix are initialized from a standard normal distribution. Similar to the input weight matrix, we connect each node inside the reservoir to a limited number of  $K^{rec} = 10$  ( $\ll N^{res}$ ) randomly selected other nodes in the reservoir, and set the remaining weights to zero. In order to fulfil the Echo State Property (ESP) that requires that the states of all reservoir neurons need to decay in a finite time for a finite input pattern, the reservoir weight matrix is normalized by its largest absolute eigenvalue and rescaled by the spectral radius  $\rho$ , because it was shown in [1] that the ESP holds as long as  $\rho < 1$ .

Together, the input scaling factor  $\alpha_u$  and the spectral radius  $\rho$  determine, how strongly the network relies on the memorized past inputs compared to the present input. These hyper-parameters need to be optimized during the training process.

Every neuron inside the reservoir receives an additional constant bias input. The bias weight vector  $w^{bi}$  with  $N^{res}$  entries is initialized by fixed random values from a uniform distribution between  $\pm 1$  and multiplied by the hyper-parameter  $\alpha_b$ . With the three weight matrices  $W^{in}$ ,  $W^{res}$  and  $w^{bi}$  the reservoir state  $r[n]$  can be computed as follows:

$$r[n] = (1 - \lambda)r[n - 1] + \lambda f_{res}(W^{in}u[n] + W^{res}r[n - 1] + w^{bi}) \quad (1)$$

Equation (1) is a leaky integration of the reservoir neurons, which is equivalent to a first-order lowpass filter. Depending on the leakage  $\lambda \in (0, 1]$ , a specific amount of the past reservoir state is leaked over time. Together with the spectral radius  $\rho$ , the leakage  $\lambda$  determines the temporal memory of the reservoir.

The reservoir activation function  $f_{res}(\cdot)$  controls the non-linearity of the system. Conventionally, the sigmoid or tanh functions are used, because their lower and upper boundaries facilitate the reservoir states stability.

The output weight matrix  $W^{out}$  has the dimensions  $N^{out} \times (N^{res} + 1)$  and connects the reservoir state  $r[n]$ , which is expanded by a constant intercept term of 1 for regression, to the output vector  $y[n]$  using Equation (2).

$$y[n] = W^{out}r[n] \quad (2)$$

Typically, the output weight matrix is computed using ridge regression. Therefore, all reservoir states calculated for the training data are concatenated into the reservoir state collection

matrix  $\mathbf{R}$ . As linear regression usually contains one intercept term, every reservoir state  $\mathbf{r}[n]$  is expanded by a constant of 1. All desired outputs  $\mathbf{d}[n]$  are collected into the output collection matrix  $\mathbf{D}$ . Then,  $\mathbf{W}^{\text{out}}$  can be computed using Equation (3), where  $\epsilon$  is the regularization parameter that needs to be tuned on a validation set.

$$\mathbf{W}^{\text{out}} = (\mathbf{R}\mathbf{R}^T + \epsilon\mathbf{I})^{-1} (\mathbf{D}\mathbf{R}^T) \quad (3)$$

The size of the output weight matrix determines the total number of free parameters to be trained in ESNs. Because linear regression can be obtained in closed form, ESNs are quite efficient and fast to train compared to typical deep-learning approaches.

### B. K-Means Clustering

In this work, we studied the frequently used  $K$ -Means algorithm [21] to improve the input weight initialization of ESNs. The  $K$ -Means algorithm groups  $N$  feature vectors  $\mathbf{u}[n]$  with  $N^{\text{in}}$  features into  $K$  clusters. Each observation is assigned to the cluster with the closest centroid, the prototype of the cluster. The basic  $K$ -Means algorithm aims to partition all  $N$  observations into  $K$  sets  $S_1, S_2, \dots, S_K$  and thereby minimizes the within-cluster sum of squares (SSE) in Equation (4):

$$\text{SSE} = \sum_{k=1}^K \sum_{\mathbf{u}[n] \in S_k} \|\mathbf{u}[n] - \mu_k\|^2. \quad (4)$$

Here,  $\mu_k$  is the centroid of the  $k$ -th set  $S_k$ , e.g. the mean of all points belonging to  $S_k$ .

In this paper, we utilized relatively large datasets. Thus, we used the fast Mini-batch  $K$ -Means algorithm proposed by Sculley et. al. [22] and initialized it based on “ $K$ -Means++” [23].

### C. Novel input weight initialization

In this paper, we propose to initialize the input weight matrix  $\mathbf{W}^{\text{in}}$  using the  $K$ -Means algorithm. To understand how a feature vector is passed to the reservoir in general, we reconsider Equation (1), which describes the computation of a new reservoir state based on the current feature vector and the previous reservoir state. For the sake of simplicity, we briefly assume a reservoir without leakage ( $\lambda = 1$ ), without any recurrent connections ( $K^{\text{rec}} = 0$ ) and with a linear activation function  $f_{\text{res}}$ . Thus, we can simplify Equation (1) to Equations (5) and (6) for the  $k^{\text{th}}$  reservoir neuron.

$$\mathbf{r}[n] = \mathbf{W}^{\text{in}} \mathbf{u}[n] \quad (5)$$

$$r_k[n] = \sum_{m=1}^{N^{\text{in}}} w_{k,m}^{\text{in}} u_m[n] = \mathbf{w}_k^{\text{in}^T} \cdot \mathbf{u}[n], \quad (6)$$

where  $m$  describes the feature index inside  $\mathbf{u}[n]$ .

This dot product is in fact closely related to the cosine similarity  $S$  in Equation (7). The only difference between Equations (6) and (7) is the normalization.

$$S = \frac{1}{\|\mathbf{w}_k^{\text{in}}\| \|\mathbf{u}[n]\|} \mathbf{w}_k^{\text{in}^T} \cdot \mathbf{u}[n] \quad (7)$$

The input weights of an ESN are responsible for passing feature vectors to the reservoir that consists of non-linear neurons. Due to the – typically – random initialization of the input weights, several relationships between different features can be computed. In this paper, we do not neglect this assumption, but we hypothesize that the main task of the input weights is to structure features according to their similarity. We also stick to the conventional linear regression-based training of ESNs, because this is a key-advantage of such networks. However, we would like to incorporate prior knowledge about the feature vectors, in an unsupervised fashion, so that it is “easier” for the ESN to solve a specific tasks.

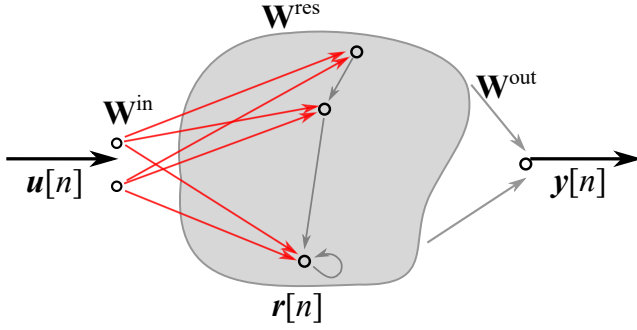
Thus, we propose to replace the randomly initialized input weights by the cluster centroids obtained from the  $K$ -means algorithm that was applied to cluster the feature vectors in  $K$  groups. The  $K$ -means algorithm detects prior structure in the feature vectors, such as phones or phone transitions speech datasets, common segments of images [24]. This way, passing feature vectors to the ESN basically consists of computing the cosine similarity between the centroids and the feature vectors.

Typically, the reservoir size  $N^{\text{res}}$  is increased after tuning the hyper-parameters using small ESNs. It has been shown that this final step significantly improves the classification results [6], [7], [25]–[27]. However, if we would simply increase the reservoir size in our novel ESN model, we needed also to increase  $K$ , as each reservoir neuron represents one cluster so far. If we increase  $K$ , we might end up with less meaningful clusters. Thus, in this paper, we propose that  $K$  does not need to be equal to  $N_{\text{res}}$ .

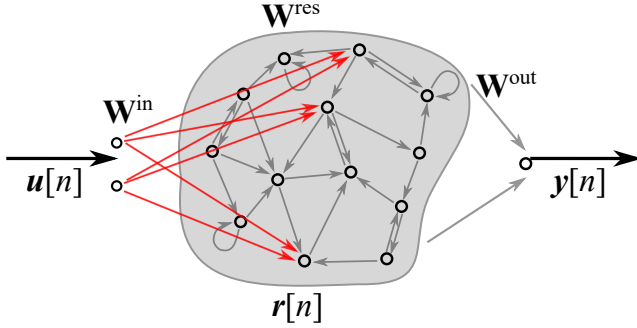
This has the advantage that we can increase  $K$  and  $N_{\text{res}}$  together, until the improvement of further increasing  $K$  gets low. Then, we can keep  $K$  constant and add additional “zero-connections” to  $\mathbf{W}^{\text{in}}$ . In that way, we ensure that the centroids are still representing useful information, and we reduce the computational complexity by using very sparse  $\mathbf{W}^{\text{in}}$  in case of large reservoirs. By padding the new input weights with a lot of “zero-connections”, we specifically limit the amount of neurons in the reservoir that receive input features. This can be compared with a cortical column in the brain that also mainly consists of recurrent connections and in which only a part of the neurons directly receives input information [28]. Thus, very large  $K$ -Means-based ESNs are even getting biologically plausible.

Figure 2 visualizes two very simple examples for the proposed  $K$ -Means-based ESN architectures. Figure 2a shows the case  $K = N^{\text{res}} = 3$ , where the number of centroids is equal to the reservoir size. Figure 2b shows the case  $K = 3$  and  $N^{\text{res}} = 13$ , where the number of centroids is much smaller than the reservoir size. As indicated by the red arrows, only a very small amount of the neurons inside the reservoir receive information directly from the input features, whilst most of

the neurons are only connected to other neurons inside the reservoir.



(a)  $K$ -Means-based ESN when  $K = N^{\text{res}} = 3$ .



(b)  $K$ -Means-based ESN when  $K < N^{\text{res}}$ .

Fig. 2. Example ESN architectures for  $K = N^{\text{res}} = 3$  (Figure 2a) and for  $K = 3$  and  $N^{\text{res}} = 13$  (Figure 2b). Only the non-zero parts of  $\mathbf{W}^{\text{in}}$  are visualized in red color. For the sparse KM-ESN, only a few neurons receive input data.

In the remainder of this paper, we refer to the basic ESN with randomly and sparsely initialized input weights as “basic ESN” and to the ESN with  $K$ -Means-based initialized input weights as “KM-ESN”. If  $N^{\text{res}} > K$ , we refer to a “sparse KM-ESN”.

### III. EXPERIMENT 1: SPOKEN DIGIT RECOGNITION

In the first experiment, we consider a classification task, namely, spoken digit recognition. We provide an extensive reservoir analysis and illustrate the impact of the  $K$ -Means clustering on the hyper-parameters.

#### A. Dataset

We used the Free Spoken Digit Dataset (FSDD) [29] that contains audio recordings for ten English isolated digits. There are in total six speakers, each of which recorded every digit 50 times. The audio files are mono WAV file with a sampling frequency of  $f_s = 8$  kHz.

FSDD is by default split into a training and test set. To optimize the hyper-parameters, we additionally split the training set into 90 % for training and 10 % for validation. All hyper-parameter optimizations were done solely on the training and validation sets.

#### B. Feature extraction

For the feature extraction, each audio file was converted to a sequence of frames using a Hann window of 32 ms with

10 ms frame shift. From each frame, 13 mel-frequency-cepstral-coefficients (MFCCs) with 50 Mel filters between 0 kHz and 4 kHz were extracted, because MFCCs are widely used and very suitable for speech recognition tasks [30]. Lastly, we normalized each feature to have zero mean and unit variance. Therefore, we calculated the mean and variance of each feature on the entire training dataset.

After extracting features from all audio files, the average sequence length in the training set was 44.5 frames for one spoken digit. In total, the training set contained 106 864 feature vectors.

#### C. Target preparation and readout post-processing

In this task, we have ten binary outputs, one for each digit from “zero” to “nine”. For each spoken digit, the target outputs were constant for all frames from the beginning to the end of the sequence (0 for inactive digits and 1 for the active digit, i.e. a one-hot encoding).

During inference, the digit scores were obtained by accumulating the digit readouts over time. The *recognised* digit is determined as the digit with the highest accumulated score over time.

#### D. Measurements

To measure the overall classification results and to optimize the hyper-parameters, the Digit Error Rate DER (8) was used.

$$\text{DER} = \frac{N_{\text{error}}}{N_{\text{samples}}}, \quad (8)$$

where  $N_{\text{error}}$  and  $N_{\text{samples}}$  were the incorrect classified digits and the overall number of digits, respectively.

#### E. Number of centroids

The key parameter of the  $K$ -means algorithm is  $K$ , the number of clusters to be used. This is strongly task-dependent and there exists no general solution for this optimization problem. One way to determine the number of centroids is to observe the summed squared error SSE for different  $K$  and to search for the point when the slope of the SSE is getting less steep. From Figure 3, where the summed squared error SSE is visualized over  $K$  for the training set, we observed that the SSE decreased very fast until  $K \approx 200$ . Afterwards, SSE still continued to decrease more slowly.

The widely used TIMIT corpus [31] includes around 50 phones. Given the dynamics within and between phones, each phone is usually considered as a multi-state model with, e.g., five states per phone. Hence, this analysis showed that the effective number of 200 clusters to some extent is in line with the total number of phone-states in the dataset. During the reservoir hyper-parameter optimization and as a trade-off between the accuracy and complexity of the model, we chose  $N_{\text{res}} = K = 100$ .

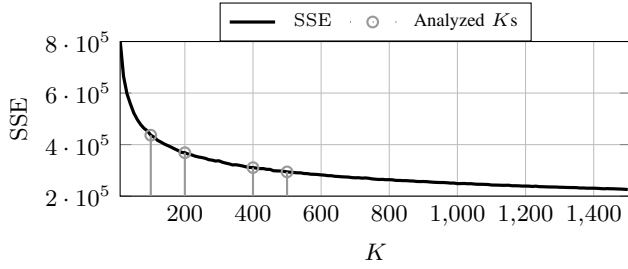


Fig. 3. Summed Squared Error (SSE) for different numbers of centroids on the FSDD dataset. A fast decrease was observed until  $K \approx 200$ . Afterwards, SSE still continued to decrease more slowly.

#### F. Optimization of the hyper-parameters of the ESNs

In Figure 4, the time signal and the extracted normalized MFCC sequence of one training example (containing the digit “zero” by the speaker Jackson) are visualized with respect to time. This serves as the running example for the following reservoir analysis.

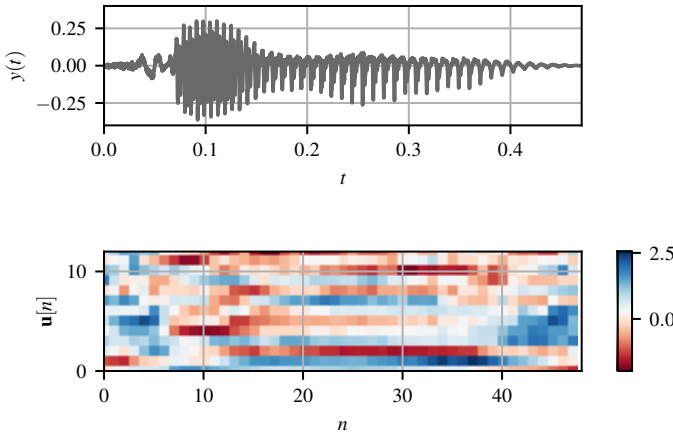


Fig. 4. Time signal and extracted normalized MFCC sequence of the digit “zero”, which was part of the training set.

In order to optimize the hyper-parameters, we began with a memory-less ESN with 100 reservoir neurons. Thus, we removed all recurrent connections (i.e.  $\rho = 0$  and  $\lambda = 1$ ). The constant bias scaling factor  $\alpha_{bi}$  was also fixed to zero.

Sweeping  $\alpha_u$  in the range of 0 to 1 while observing the Digit Error Rate DER led to an input scaling of 0.4 for the basic ESN and an input scaling of 0.8 for the KM-ESN. This indicated that for low input scaling factors, the neurons in the KM-ESN are less activated than in the basic ESN. An increased input scaling factor compensates this and leads to a higher activation of the reservoir neurons.

In Figure 5, 50 randomly selected reservoir states out of 100 states of both ESNs are visualized over time. In Figure 5a, the states of many neurons in the basic ESN showed a similar activation across different neurons. Some states seem to follow the MFCC sequence from Figure 4. However, many states did not necessarily represent the temporal dynamics of the input feature.

When we compare this to the reservoir states of the KM-ESN in Figure 5b, we observe various differences: In many

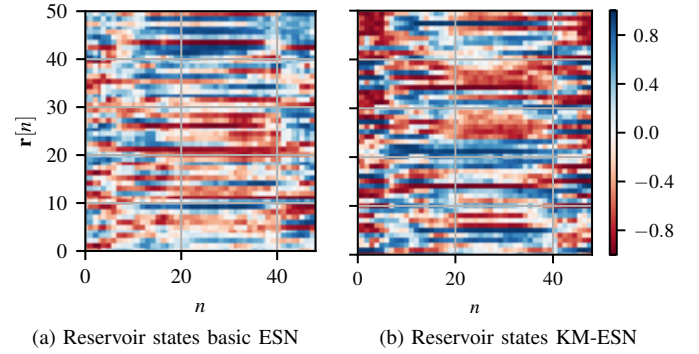


Fig. 5. Reservoir states and histograms of reservoir activations for the basic ESN and for the KM-ESN with the optimized input scaling values.

time steps, a few neurons had a remarkably high activation and work in the non-linear zone of  $\tanh$ , while most of the other neurons showed a similar behaviour as in case of the basic ESN. Interestingly, the state dynamics were similar to the dynamics of the MFCC sequence.

These observations are the consequences of the proposed  $K$ -Means-based weight initialization algorithm. Given that each neuron in the reservoir was associated to one cluster and assuming that the feature vectors of each sample (digit) belong to a fraction of clusters, it would be logical to expect that only a few neurons are strongly excited for one digit. Thus, the feature vector and the specific centroid showed in similar directions.

Recalling the hypothesis that the  $K$ -Means algorithm learns different states of phones and that the utterance “zero” consists of four or five phones, a smaller group of highly activated neurons supports the hypothesis that the  $K$ -Means algorithm really learns states of phones.

The next hyper-parameter to be optimized was the leakage  $\lambda$ . We did a line search to optimize this parameter, which is the coefficient of a first-order lowpass filter [32], and controls the “leakage” rate of the past state of each neuron to that neuron over time.

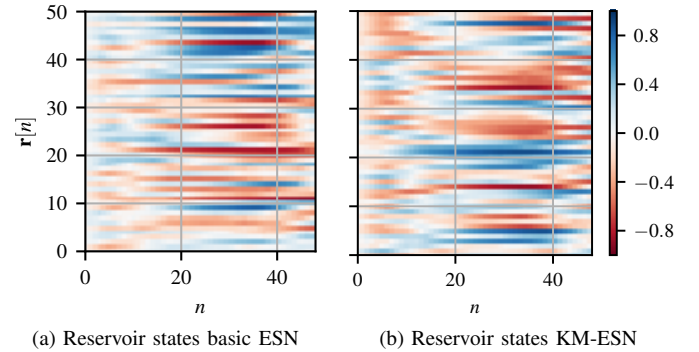


Fig. 6. Reservoir states for the basic ESN and for the KM-ESN with the optimized leakage rate  $\lambda$ .

We determined  $\lambda = 0.1$  as the ideal value for both the basic ESN and the KM-ESN. This relatively low value was reasonable as the target outputs were constant for the entire digit. Thus, the DER benefits from very smooth reservoir states. In Figure



6, the reservoir states after optimizing  $\lambda$  are visualized. As expected, the reservoir trajectories are much smoother now. Particularly in Figure 6b we observed that several neurons had very high activations compared to the basic ESN in Figure 6a, where more neurons had similar activations. As the all reservoir states are smoothed by the leakage in exactly the same way, the reservoir states now are a smoothed variant of the ones after optimizing  $\alpha_u$ .

The next hyper-parameter to optimize was the spectral radius  $\rho$ . Sweeping  $\rho$  in the range of 0 to 1 leads to the optimal value  $\rho = 1.0$  for the basic ESN, and  $\rho = 0.4$  for the KM-ESN.

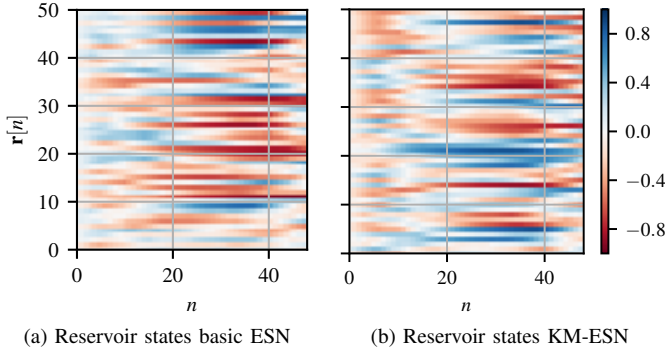


Fig. 7. Reservoir states for the basic ESN and for the KM-ESN with the optimized spectral radius  $\rho$ .

The spectral radius determines the strength of the recurrent weights. Due to the previously optimized input scaling, we have already introduced a lot of variance in the reservoir state in case of the KM-ESN. Thus, the KM-ESN benefited less from additional variance by the reservoir states. The visualization of the reservoir states in Figure 7b is very similar to Figure 6b after optimizing the leakage. However, the basic ESN needed a stronger spectral radius to obtain reservoir states with a larger variance. If we compare Figure 7a and 7b, we can see that the reservoir states of the basic ESN and of the KM-ESN were much more similar after optimizing the spectral radius.

Finally, we optimized  $\alpha_{bi}$ , the scaling of the constant bias input for every neuron, using a parameter sweep from 0 to 1. Bias adds to the non-linearity of the system by shifting the relaxed state of neurons towards the non-linear zones of the activation function. In our experiments we did not observe significant changes in the performance of the ESNs, meaning that more non-linearity was not required and  $\alpha_{bi} = 0$ .

### G. Impact of the reservoir size

As mentioned in the introduction, ESNs typically benefit from increasing the reservoir size after fixing the other hyper-parameters. At the same time, we were reluctant to add to the complexity of the  $K$ -Means model by increasing  $K$  as much as  $N_{res}$ . Therefore, we only increased  $K$  and  $N_{res}$  up to 500 and from that point we only increased the reservoir size while  $K = 500$ . This means that the input layers of the ESNs were fully connected until  $N_{res} = 500$  and for all the larger models, the input features were connected to only 500 reservoir nodes (i.e. sparse input connections). Therefore we also repeated

the hyper-parameter optimization for these sparsely connected KM-ESNs.

The optimized hyper-parameters for the new initialized ESNs are summarized in Table I. This resulted in smaller input scaling and larger spectral radius. As the impact of the randomly initialized reservoir weights increases with more reservoir neurons, we can see that the hyper-parameters of the large KM-ESN got more similar to those of the basic ESN.

TABLE I  
OPTIMIZED HYPER-PARAMETERS FOR THE BASIC ESN, SMALL KM-ESN ( $N_{res} < 500$  AND DENSE INPUT LAYER) AND LARGE KM-ESN ( $N_{res} > 500$  AND SPARSE INPUT LAYER).

Parameter	Basic ESN	KM-ESN	
		dense	sparse
Input scaling $\alpha_u$	0.4	0.8	0.2
Leakage $\lambda$	0.1	0.1	0.1
Spectral radius $\rho$	1.0	0.4	0.6
Bias scaling $\alpha_{bi}$	0.0	0.0	0.0

In Figure 8, the final DER computed on the training and test sets for different reservoirs are visualized. The training and test DER of the basic ESNs were in a similar range. The training DER of the KM-ESN was slightly larger than the test DER, especially for very small reservoir sizes.

In case of small reservoir sizes, the KM-ESN performed much better than the basic ESN, whereas in case of very large ESN models the performance became more similar. However, it can be noticed that the KM-ESN needed only 3000 neurons to reach the final test DER of 0%, whereas the DER of the KM-ESN decreased to 0% in case of the ESN with 4000 neurons.

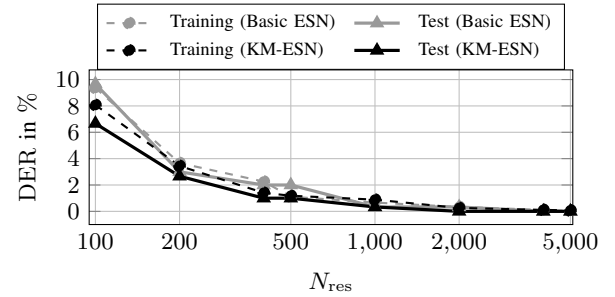


Fig. 8. Digit Error Rate (DER) for different reservoir sizes. KM-ESN performs equally well or better than the basic ESN for all reservoir sizes.

In general, both ESNs performed well on this tasks, while the KM-ESN achieved better results than the basic ESN in almost all cases.

### H. Robustness against random initializations

In order to study the robustness of ESN against initialization, we initialized and trained both the basic ESN and the KM-ESN ( $N_{res} = 100$ ) 20 times. In Table II the minimum, maximum and mean DER for a basic ESN and for the KM-ESN model are summarized. KM-ESN not only outperformed the basic ESN, but also demonstrated less variation compared to the basic ESN.

TABLE II

min, max AND MEAN DER FOR A BASIC ESN AND FOR THE KM-ESN. ALL MODELS WERE INITIALIZED, TRAINED AND EVALUATED 20 TIMES. THE KM-ESN ACHIEVED LOWER DER WITH LESS VARIATION COMPARED TO THE BASIC ESN.

	DER (random ESN)		DER (KM-ESN)	
	Training	Test	Training	Test
min	8.30 %	6.00 %	6.19 %	5.33 %
max	10.93 %	12.33 %	9.26 %	10.00 %
Mean	9.54 %	8.80 %	8.03 %	7.30 %

#### IV. EXPERIMENT 2: FUNDAMENTAL FREQUENCY EXTRACTION

In this section we focus on the  $f_0$  extraction with ESNs, an interesting problem which is a combination of classification and regression subtasks.

We particularly investigated the impact of very large reservoirs with up to 20 000 neurons. This could not be covered well in the relatively simple task of isolated digit recognition, due to the small dataset.

##### A. Dataset

We used the Pitch Tracking dataset PTDB-TUG [33] that consists of 4720 sentences from 20 speakers (10 male and 10 female) of read speech. The audio files are 4720 mono WAV files with a sampling frequency of  $f_s = 48$  kHz.

In [34], [35], a split in training, validation and test sets was proposed. Although the exact split is not publicly available to the best of our knowledge, we can still adopt their strategy. We used the speakers F01-F08 and M01-M08 (16 speakers in total) as the training set. From each speaker in the training set, we randomly selected 36 utterances (576 sentences in total) to be used as a validation set to tune the hyper-parameters with. All files from the remaining four speakers F09-F10 and M09-M10 were used as a test set with unknown speakers.

##### B. Feature extraction

For this experiment, we used relatively large feature vectors. We converted each audio file to a sequence of frames (with 40 ms length and 30 ms overlap). From each frame, short-term spectra were extracted with a Hann window of length 2048. We dropped high-frequency contents above 1.5 kHz as they do not carry important  $f_0$  information. This led to 65 frequency bins in total. To enrich the temporal context, we appended the preceding and following two spectra to the current spectrum and thus had a feature vector size of  $5 \times 65 = 325$ . Finally, we applied the log function after adding an  $\epsilon = 1$  to every feature.

After extracting features for all samples, the average sequence length in the training set was 740 frames for one sentence. In total, the training set contained 2,366,160 feature vectors.

##### C. Target preparation and readout post-processing

In this task, the model had two outputs. The first output was binary and indicated voiced (1) and unvoiced (0) speech segments. The second output was continuous and its target value was either the  $f_0$  value in a frame or 0 in case of unvoiced frames.

During the inference, the first output was binarized to 0 and 1 by setting a threshold of 0.5. The final output was then the product of the binarized output and the continuous regression output in each time step.

##### D. Measurements

The  $f_0$  extraction can be defined as a combination of a binary voiced-unvoiced classification and a regression task to compute the actual  $f_0$  in Hz of voiced speech. From this point of view, several standard error measures for the evaluation of  $f_0$  extraction are defined in [36].

The first error measure is the Gross Pitch Error (GPE) in Equation (9), which is the proportion of frames that are considered voiced by both pitch tracker and ground truth ( $N_{VV}$ ), where the relative pitch error is higher than 20 % ( $N_{f_0E}$ ).

$$\text{GPE} = \frac{N_{f_0E}}{N_{VV}} \quad (9)$$

In addition, we evaluated the precision of the computed  $f_0$  values in the correctly voiced frames. Therefore, we used the Fine Pitch Error (FPE), which is the standard deviation of the distribution of relative error values (in cents) from the frames that do not have gross pitch errors. This can be treated as a regression metric.

##### E. Optimization of the hyper-parameters of the ESNs

The optimization of the ESN models for  $f_0$  extraction followed exactly the same way as introduced in Section III-F. The determined hyper-parameters of the models are summarized in Table III. During the optimization, the Gross Pitch Error GPE dropped from 34.3 % to 30 % in case of a basic ESN with  $N_{res} = 500$ . A KM-ESN of the same reservoir size and  $K = 500$ , showed the drop in GPE from 24.3 % to 20.5 %.

TABLE III  
OPTIMIZED HYPER-PARAMETERS FOR THE BASIC ESN AND FOR THE KM-ESN WITH SMALL AND INCREASED RESERVOIR SIZES.

Parameter	random	KM-ESN	
		small	large
Input scaling $\alpha_{in}$	0.6	0.1	0.1
Spectral radius $\rho$	0.6	0.1	0.4
Bias scaling $\alpha_{bi}$	0.6	2.1	0.4
Leakage $\lambda$	0.5	1.0	1.0

Figure 9 shows an example validation readout for both, basic ESN and KM-ESN. In this particular example, the basic ESN achieved the lowest validation GPE. From Figure 9a can be observed that the basic ESN very often missed its target value, e.g. between  $n = 270$  and  $n = 290$  or between  $n = 420$  and

$n = 440$ . In contrast to that, the KM-ESN in 9b achieved a more smoothed  $f_0$  trajectory. Of course, also here we can see difficulties, such as from  $n = 360$  to  $n = 370$  or between  $n = 420$  and  $n = 440$ . Both, basic ESN and the KM-ESN show difficulties for voiced-unvoiced transitions, e.g. from  $n = 330$  to  $n = 360$ .

#### F. Error analysis

In Figure 10a, the Gross Pitch Error Rate (GPE) is visualized for different reservoir sizes and for the training and test sets. Especially the basic ESN models significantly benefited from large reservoir sizes. The best performance was achieved with a basic ESN model with 10k reservoir neurons, when the GPE decreased from 51.1 % to 27.4 %. A marginal overfitting was observed mostly for too large reservoir. Similar behaviour has also been reported in other publications and applications, such as [7], [26], [27].

In case of KM-ESN, we increased both the reservoir size and the number of clusters together until  $N_{res} = K = 500$ , hence, the inputs were fully connected to the reservoir nodes. For larger reservoirs, we kept the number of clusters fixed to  $K = 500$ . Therefore in those models, only 500 reservoir nodes were connected to the input features.

It is remarkable that a small KM-ESN with only 300 nodes had the same performance (GPE = 27.4 %) as a basic ESN with even 10k nodes. Afterwards, the behavior of KM-ESN improved more slowly to minimum GPE = 25 % for 5k neurons. We argue our proposed unsupervised input weight initialization supplied the input features to the reservoir more efficiently so that a small reservoir could extract the same information as a much larger reservoir with random input weights.

Figure 10b shows the Fine Pitch Error Rate (FPE) in cents for different reservoir architectures. This allowed us to analyze the regression capabilities of the different models. In this experiment, the best basic ESN (with 5k nodes) is inferior to any KM-ESN with a minimum of 200 nodes. Note that for the fine pitch evaluation we used the same models that were optimized with GPE metric.

#### G. Computational complexity

So far, we have shown that very small KM-ESNs have outperformed large basic ESNs. The GPE as well as the FPE of a KM-ESN with 300 was competitive or better than of a basic ESN with 10 000 neurons.

Finally, we analyzed the computational complexity of the different models using the training set of the PTDB-TUG dataset, which has around 394 min of recorded audio. From Table IV we noticed that all best performing models were trained and tested faster than real-time, measured on one 2.5 GHz core. The small KM-ESN was much faster in training and inference than the basic ESN with 8000 neurons.

For all ESN models, the training time included online feature extraction, collecting sufficient statistics for each feature vector sequence, and finally computing the output weights.

The  $K$ -Means training was an additional step that needed to be performed before the ESN training. This included extracting

TABLE IV  
TIME MEASUREMENT FOR DIFFERENT ESN ARCHITECTURES. THE TRAINING AND INFERENCE TIME FOR THE BASIC ESN CAN DIRECTLY BE TAKEN FROM THE TABLE. THE TRAINING TIME FOR THE KM-ESN WITH 300 NEURONS IS THE SUM OF THE TIME FOR OFFLINE FEATURE EXTRACTION,  $K$ -MEANS TRAINING AND ESN TRAINING. THESE TWO STEPS ARE ONLY REQUIRED DURING THE TRAINING AND NOT FOR INFERENCE.

Step	Training time	Inference time
Basic ESN (8000 neurons)	127 min	58 min
Feature extraction for $K$ -Means	2.2 min	–
$K$ -Means ( $K = 300$ )	6.5 min	–
KM-ESN (300 neurons)	8.1 min	7.9 min

all feature vectors from the training set followed by training the  $K$ -Means model. In total KM-ESN with 300 neurons took 14.6 min compared to, for example, 127 min training time for a basic ESN of 8000 neurons.

The inference time for both ESN models included online feature extraction, computing reservoir states and finally computing outputs for each feature vector sequence. Note that in Table IV the inference time for the basic ESN with 8000 neurons was 58 min compared to only 7.9 min for the small KM-ESN model with 300 neurons. As the  $K$ -Means centroids were used as the input weights of the ESN model, we did not have any additional computational complexity during inference.

#### V. CONCLUSIONS AND OUTLOOK

We presented an efficient way to initialize the input weights of Echo State Networks using the unsupervised  $K$ -Means algorithm. Motivated by the fact that passing feature vectors to a reservoir neuron is closely related to the cosine similarity, we used the centroids of the  $K$ -Means algorithm as input weights. This had the effect that the neuron activation was high only if the feature vector and a centroid were similar. Most of the neuron activations were relatively low. We showed that a particular difference occurred in several neurons with a large variance, which supported the hypothesis that the  $K$ -Means algorithm indeed supplied the KM-ESN with beneficial information about the dataset.

We showed that the KM-ESN model outperformed basic ESNs in two experiments – spoken digit recognition and  $f_0$  extraction. For spoken digit recognition, the  $K$ -Means-based ESN was more robust compared to random initialization. In case of  $f_0$  extraction, the novel ESN model was more accurate as the FPE was much lower than for randomly initialized models.

As the weight initialization was both data-driven and unsupervised, we postulate that we can use exactly the same input weights for any task on the same dataset. For example, if we would have a phonemic transcription of the FSDD, we could easily perform phoneme recognition without changing the  $K$ -Means algorithm in any way. The only required change is to tune hyper-parameters accordingly, and to train another set of output weights. In addition, as the  $K$ -Means algorithm does not need any labelled data, we can, for example, easily



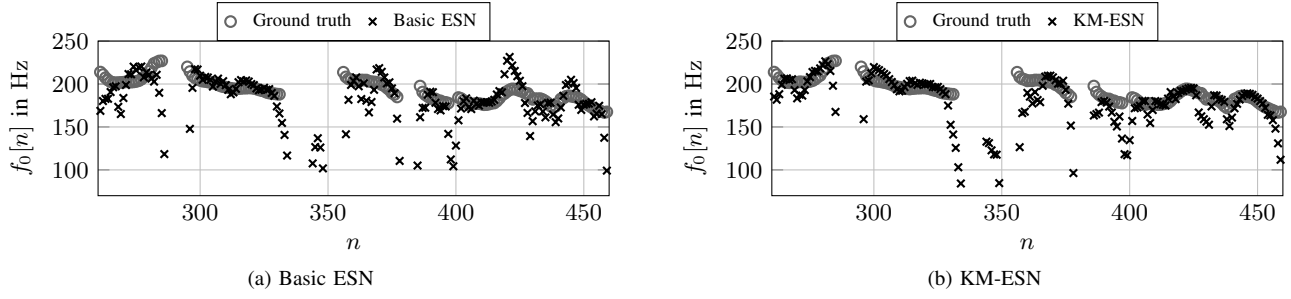


Fig. 9. Example validation readout of the basic ESN and the KM-ESN. The readout of the KM-ESN has a smoother trajectory, although no leaky integration was required here.

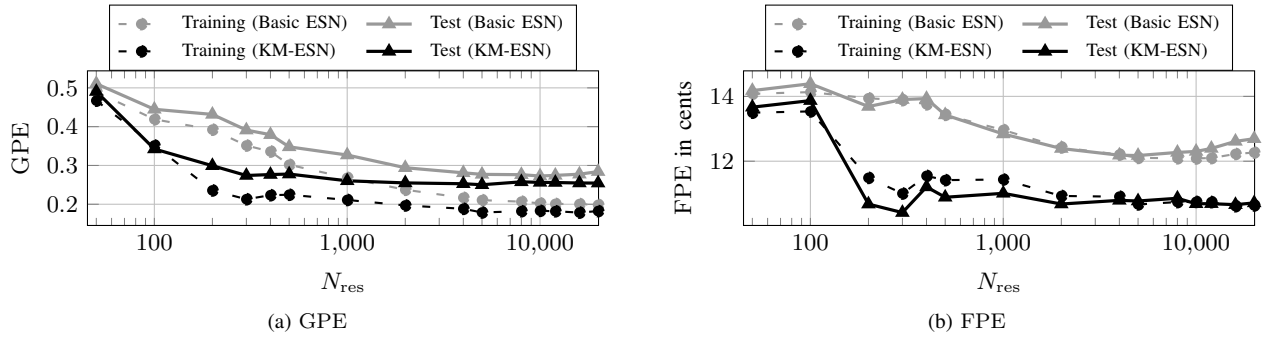


Fig. 10. Gross Pitch Error (GPE) and Fine Pitch Error (FPE) for different reservoir sizes. Even a small KM-ESN model with 300 nodes performs as well as a very large basic ESN with 10k nodes in terms of GPE and FPE.

extend the given FSDD with additional recordings from other speakers without needing labels. This can help the KM-ESN to generalize towards unknown speakers.

A remarkable advantage of the novel ESN model is definitely the few required free parameters: Basically, already with a reservoir size of 200, we achieved comparable results to a conventional ESN of 10000 nodes in case of  $f_0$  extraction.

In the future, we will analyze the capability of the proposed technique to solve more challenging tasks, such as phoneme recognition or multipitch tracking in music signals. It will also be interesting to determine the capability of predicting time-series. We will also investigate ways to pre-train the reservoir weights. If this is possible completely data-driven, we could remove further randomness of ESNs.

Code examples for the two experiments are publicly available in our Github repository (<https://github.com/TUD-STKS/PyRCN/>).

## REFERENCES

- [1] H. Jaeger, "The "echo state" approach to analysing and training recurrent neural networks," German National Research Center for Information Technology, Tech. Rep. GMD Report 148, 2001. [Online]. Available: <http://www.faculty.iu-bremen.de/hjaeger/pubs/EchoStatesTechRep.pdf>
- [2] M. C. Ozturk, D. Xu, and J. C. Principe, "Analysis and Design of Echo State Networks," *Neural Computation*, vol. 19, no. 1, pp. 111–138, 2007. [Online]. Available: <https://doi.org/10.1162/neco.2007.19.1.111>
- [3] M. Lukoševičius, H. Jaeger, and B. Schrauwen, "Reservoir Computing Trends," *KI – Künstliche Intelligenz*, vol. 26, no. 4, pp. 365–371, 2012.
- [4] S. Scardapane and D. Wang, "Randomness in neural networks: an overview," *WIREs Data Mining and Knowledge Discovery*, vol. 7, no. 2, p. e1200, 2017. [Online]. Available: <https://onlinelibrary.wiley.com/doi/abs/10.1002/widm.1200>
- [5] Y. Xue, L. Yang, and S. Haykin, "Decoupled echo state networks with lateral inhibition," *Neural Networks*, vol. 20, no. 3, pp. 365 – 376, 2007, echo State Networks and Liquid State Machines. [Online]. Available: <http://www.sciencedirect.com/science/article/pii/S0893608007000378>
- [6] A. Jalalvand, F. Triefenbach, K. Demuyneck, and J.-P. Martens, "Robust continuous digit recognition using Reservoir Computing," *Computer Speech & Language*, vol. 30, no. 1, pp. 135 – 158, 2015.
- [7] A. Jalalvand, K. Demuyneck, W. D. Neve, and J.-P. Martens, "On the application of reservoir computing networks for noisy image recognition," *Neurocomputing*, vol. 277, pp. 237 – 248, 2018, hierarchical Extreme Learning Machines.
- [8] A. Rodan and P. Tino, "Minimum Complexity Echo State Network," *IEEE Transactions on Neural Networks*, vol. 22, no. 1, pp. 131–144, Jan 2011.
- [9] T. Strauss, W. Wustlich, and R. Labahn, "Design Strategies for Weight Matrices of Echo State Networks," *Neural Computation*, vol. 24, no. 12, pp. 3246–3276, 2012, pMID: 22970872. [Online]. Available: [https://doi.org/10.1162/NECO\\_a\\_00374](https://doi.org/10.1162/NECO_a_00374)
- [10] A. Griffith, A. Pomerance, and D. J. Gauthier, "Forecasting chaotic systems with very low connectivity reservoir computers," *Chaos: An Interdisciplinary Journal of Nonlinear Science*, vol. 29, no. 12, p. 123108, 2019. [Online]. Available: <https://doi.org/10.1063/1.5120710>
- [11] T. L. Carroll and L. M. Pecora, "Network structure effects in reservoir computers," *Chaos: An Interdisciplinary Journal of Nonlinear Science*, vol. 29, no. 8, p. 083130, 2019. [Online]. Available: <https://doi.org/10.1063/1.5097686>
- [12] L. Appeltant, M. C. Soriano, G. V. der Sande, J. Danckaert, S. Massar, J. Dambre, B. Schrauwen, C. R. Mirasso, and I. Fischer, "Information processing using a single dynamical node as complex system," *Nature communications*, vol. 2, no. 1, pp. 1–6, 2011.
- [13] M. Lukoševičius, "On self-organizing reservoirs and their hierarchies," 2010.
- [14] S. Basterrech, C. Fyfe, and G. Rubino, "Self-Organizing Maps and Scale-Invariant Maps in Echo State Networks," in *2011 11th International Conference on Intelligent Systems Design and Applications*, Nov 2011, pp. 94–99.
- [15] S. Basterrech and V. Snášel, "Initializing Reservoirs with Exhibitory and Inhibitory Signals Using Unsupervised Learning Techniques," in *Proceedings of the Fourth Symposium on Information and*

- Communication Technology*, ser. SoICT '13. New York, NY, USA: Association for Computing Machinery, 2013, pp. 53–60. [Online]. Available: <https://doi.org/10.1145/2542050.2542087>
- [16] A. Lazar, G. Pipa, and J. Triesch, “SORN: a self-organizing recurrent neural network,” *Frontiers in Computational Neuroscience*, vol. 3, p. 23, 2009. [Online]. Available: <https://www.frontiersin.org/article/10.3389/neuro.10.023.2009>
  - [17] B. Schrauwen, M. Wardermann, D. Verstraeten, J. J. Steil, and D. Stroobandt, “Improving reservoirs using intrinsic plasticity,” *Neurocomputing*, vol. 71, no. 7, pp. 1159 – 1171, 2008, progress in Modeling, Theory, and Application of Computational Intelligence. [Online]. Available: <http://www.sciencedirect.com/science/article/pii/S0925231208000519>
  - [18] W. M. Ashour, A. S. Abu-Issa, and O. Hellwich, “Clustering Algorithms in Echo State Networks,” *International Journal of Signal Processing, Image Processing and Pattern Recognition*, vol. 9, no. 5, pp. 15–24, 2016.
  - [19] W. Barbakh and C. Fyfe, “ONLINE CLUSTERING ALGORITHMS,” *International Journal of Neural Systems*, vol. 18, no. 03, pp. 185–194, 2008, pMID: 18595148. [Online]. Available: <https://doi.org/10.1142/S0129065708001518>
  - [20] —, “Local vs global interactions in clustering algorithms: Advances over K-means,” *International Journal of Knowledge-based and Intelligent Engineering Systems*, vol. 12, no. 2, pp. 83–99, 2008.
  - [21] S. Lloyd, “Least squares quantization in PCM,” *IEEE Transactions on Information Theory*, vol. 28, no. 2, pp. 129–137, March 1982.
  - [22] D. Sculley, “Web-scale k-means clustering,” in *Proceedings of the 19th international conference on World wide web*, 2010, pp. 1177–1178.
  - [23] D. Arthur and S. Vassilvitskii, “K-means++: the advantages of careful seeding,” in *Proceedings of the eighteenth annual ACM-SIAM symposium on Discrete Algorithms*. Society for Industrial and Applied Mathematics Philadelphia, PA, USA, 2007, pp. 1027–1035.
  - [24] A. Coates, A. Ng, and H. Lee, “An Analysis of Single-Layer Networks in Unsupervised Feature Learning,” in *Proceedings of Machine Learning Research*, G. Gordon, D. Dunson, and M. Dudík, Eds., vol. 15. Fort Lauderdale, FL, USA: JMLR Workshop and Conference Proceedings, 11–13 Apr 2011, pp. 215–223. [Online]. Available: <http://proceedings.mlr.press/v15/coates11a.html>
  - [25] F. Triefenbach, A. Jalalvand, B. Schrauwen, and J. pierre Martens, “Phoneme Recognition with Large Hierarchical Reservoirs,” in *Advances in Neural Information Processing Systems 23*. Curran Associates, Inc., 2010, pp. 2307–2315. [Online]. Available: <http://papers.nips.cc/paper/4056-phoneme-recognition-with-large-hierarchical-reservoirs.pdf>
  - [26] P. Steiner, S. Stone, P. Birkholz, and A. Jalalvand, “Multipitch tracking in music signals using Echo State Networks,” in *2020 28th European Signal Processing Conference (EUSIPCO)*, 2020, pp. 126–130. [Online]. Available: <https://www.eurasip.org/Proceedings/Eusipco/Eusipco2020/pdfs/0000126.pdf>
  - [27] P. Steiner, A. Jalalvand, S. Stone, and P. Birkholz, “Feature Engineering and Stacked Echo State Networks for Musical Onset Detection,” in *2020 25th International Conference on Pattern Recognition (ICPR)*, 2020, pp. 9537–9544.
  - [28] W. Maass, “Liquid state machines: motivation, theory, and applications,” *Computability in context: computation and logic in the real world*, pp. 275–296, 2011.
  - [29] Z. Jackson, C. Souza, J. Flaks, Y. Pan, H. Nicolas, and A. Thite, “Jakobovski/free-spoken-digit-dataset: v1.0.8,” Aug. 2018. [Online]. Available: <https://doi.org/10.5281/zenodo.1342401>
  - [30] R. Vergin, D. O’Shaughnessy, and A. Farhat, “Generalized mel frequency cepstral coefficients for large-vocabulary speaker-independent continuous-speech recognition,” *IEEE Transactions on Speech and Audio Processing*, vol. 7, no. 5, pp. 525–532, Sep. 1999.
  - [31] J. S. Garofolo, L. F. Lamel, W. M. Fisher, J. G. Fiscus, and D. S. Pallett, “DARPA TIMIT acoustic-phonetic continuous speech corpus CD-ROM. NIST speech disc 1-1.1,” *NASA STI/Recon Technical Report N*, p. 27403, 2 1993.
  - [32] H. Jaeger, M. Lukoševičius, D. Popovici, and U. Siewert, “Optimization and applications of echo state networks with leaky- integrator neurons,” *Neural Networks*, vol. 20, no. 3, pp. 335 – 352, 2007, echo State Networks and Liquid State Machines.
  - [33] G. Pirker, M. Wohlmayr, S. Petrik, and F. Pernkopf, “A Pitch Tracking Corpus with Evaluation on Multipitch Tracking Scenario,” in *INTERSPEECH 2011*, 2011, pp. 1509–1512. [Online]. Available: [https://www.isca-speech.org/archive/interspeech\\_2011/i11\\_1509.html](https://www.isca-speech.org/archive/interspeech_2011/i11_1509.html)
  - [34] A. Kato and T. Kinnunen, “Waveform to Single Sinusoid Regression to Estimate the F0 Contour from Noisy Speech Using Recurrent Deep Neural Networks,” in *Proc. Interspeech 2018*, 2018, pp. 327–331. [Online]. Available: <http://dx.doi.org/10.21437/Interspeech.2018-1671>
  - [35] —, “A Regression Model of Recurrent Deep Neural Networks for Noise Robust Estimation of the Fundamental Frequency Contour of Speech,” in *Proc. Odyssey 2018 The Speaker and Language Recognition Workshop*, 2018, pp. 275–282. [Online]. Available: <http://dx.doi.org/10.21437/Odyssey.2018-39>
  - [36] S. Strömbergsson, “Today’s Most Frequently Used F0 Estimation Methods, and Their Accuracy in Estimating Male and Female Pitch in Clean Speech,” in *Interspeech 2016*, 2016, pp. 525–529. [Online]. Available: <http://dx.doi.org/10.21437/Interspeech.2016-240>